Spin–orbit autoionization and intensities in the double-resonant delayed pulsed-field threshold photoionization of HCl

Y.-F. Zhu, E. R. Grant, Kwanghsi Wang, V. McKoy, and H. Lefebvre-Brion

Citation: The Journal of Chemical Physics **100**, 8633 (1994); doi: 10.1063/1.466717
View online: http://dx.doi.org/10.1063/1.466717
View Table of Contents: http://scitation.aip.org/content/aip/journal/jcp/100/12?ver=pdfcov
Published by the AIP Publishing

Spin–orbit autoionization and intensities in the double-resonant delayed pulsed-field threshold photoionization of HCl

Y.-F. Zhu and E. R. Grant
Department of Chemistry, Purdue University, West Lafayette, Indiana 47907

Kwanghsi Wang and V. McKoy
Arthur Amos Noyes Laboratory of Chemical Physics, California Institute of Technology, Pasadena, California 91125

H. Lefebvre-Brion
Laboratoire de Photophysique Moléculaire, Bâtiment 213, Université de Paris-Sud 91405, Orsay, France

(Received 16 November 1993; accepted 28 February 1994)

State-selected delayed pulsed-field threshold photoionization spectra of HCl and DCl are recorded in double-resonant transitions through the $F\ ^1\Delta$, $E\ ^1\Sigma^+$, and $g\ ^3\Sigma^-$ states of the $4p\pi$ Rydberg configuration. Comparison of observed rotational line strengths with calculated spectra, as well as with available time-of-flight photoelectron spectra, provides useful insight on the influence of spin–orbit and rotational autoionization on delayed pulsed-field threshold photoionization of HCl. Spin–orbit and rotational autoionization are seen to dramatically reduce the ion rotational intensity associated with the upper spin–orbit level of the ion.

I. INTRODUCTION

The electronic structure underlying the higher excited states of HCl has been a subject of significant experimental and theoretical attention. Early extensive characterization of rovibrational structure in Rydberg and valence states over the interval within 25 000 cm^{-1} of the ionization limit[1] has provided an extensive map of potential curves perturbed by spin–orbit and Rydberg-valence coupling which has stimulated high-level calculations.[2] More recently, laser multiphoton spectroscopy has sharpened assignments[3,4] and probed the dynamical consequences of relaxation via predissociation and ion-pair formation.[5,6]

Above the first ionization threshold, structure in the spectrum of autoionizing resonances can be analyzed to establish convergence limits of Rydberg series and provide information on the dynamics of coupling between electronic and core internal degrees of freedom, particularly spin–orbit coupling between bound Rydberg states and the ionization continuum. Experimental work at Purdue has applied methods of double-resonance spectroscopy to resolve rotational structure in these spin–orbit autoionizing Rydberg series to within a few tens of wave numbers of the $^2\Pi_{1/2}$ ionization threshold.[7,8] In this way, ionization-detected absorption scans from intermediate two-photon selected levels of the $4p\pi$ $F\ ^1\Delta$ Rydberg state have yielded spectra characterizing numerous autoionizing series with rotational structure spanning the range between Hund's case (c) and (e) limits of core-Rydberg orbital angular momentum coupling. In related work, we have applied the same excitation scheme to obtain rotationally resolved double-resonance threshold photoionization spectra.[8] These spectra, recorded in transitions from an unperturbed intermediate Rydberg state, have motivated *ab initio* calculations of state-specific photoionization cross sections.[9]

More recently, de Beer *et al.*[10] have systematically characterized final-state distributions in (2+1) photoionizing transitions of HCl via the same intermediate state, using conventional time-of-flight photoelectron spectroscopy in which they were able to resolve spin–orbit and rotational structure. Comparing these distributions to the relative intensities of transitions to the same final states observed both by de Beer *et al.*[10] and by us using delayed pulsed-field threshold ionization spectroscopy, they conclude that autoionization and rotational coupling significantly affect the observed intensities in delayed pulsed-field threshold photoionizations by perturbing the lifetimes of near-threshold Rydberg states. The possible effect of autoionization on delayed threshold photoionization intensities in HCl was also noted by Lefebvre-Brion,[11] and discussed in a review by Merkt and Softley.[12] Similar effects have been proposed to explain line strengths in XUV threshold photoionization of CO_2.[13]

In the present work, we explore this issue in further depth for HCl by investigating double-resonant threshold photoionization spectra using a set of intermediate states for which we have performed *ab initio* calculations of threshold photoionization intensities. We revisit the $F\ ^1\Delta$ state, recording threshold photoionization spectra for $J'=2$ and 3 in DCl. In addition, we examine new intermediate states, $E\ ^1\Sigma^+$ and $g\ ^3\Sigma^-$, which are both nominally Rydberg but differ from the $F\ ^1\Delta$ state by having low electronic angular momentum and perturbative interactions with the valence $V\ ^1\Sigma^+$ state. We compare intensities observed in each case with calculated cross sections obtained using *ab initio* transition moments for direct photoionization of selected intermediate states to the manifold of ion rotational states. Comparison of theory with experiment illustrates the importance of the electronic character of the intermediate state in concert with final state dynamics as factors determining rotationally resolved delayed pulsed-field threshold photoionization intensities.

II. EXPERIMENT

Threshold photoionization resonances of HCl and DCl are observed by two-color double-resonant excitation accompanied by delayed pulsed-field threshold photoelectron

 0021-9606/94/100(12)/8633/8/$6.00

detection[14] under molecular beam conditions. The beam originates from a pulsed jet of HCl seeded 10% in He or neat DCl, which is skimmed and expanded into the extraction region of a delayed pulsed-field threshold photoionization spectrometer by passing through a grid on the first element (repeller) of a three-element ion-optics assembly. The second (extractor) and third (entrance) elements also hold grids.

Between the repeller and extractor the molecular beam is crossed by counterpropagating outputs of a pair of pulsed dye lasers (Lambda Physik FL2002), overlapped in time and space and each focused by a 50 cm f.l. lens. The dye lasers are pumped by the output of a single Lambda Physik EMG201 MSC XeCl excimer laser. The first dye laser provides pulse energies from 5 to 15 mJ at selected frequencies in the visible, which are doubled in BBO to yield filtered UV output on the order of 1 mJ. This output initiates double resonance via two-photon transitions to selected levels of the $F\ ^1\Delta$, $E\ ^1\Sigma^+$, and $g\ ^3\Sigma^-$ electronic states, all of which arise from the $4p\pi$ Rydberg configuration. The second laser, pumped to produce visible pulses of around 1 mJ, is then scanned to probe subsequent transitions to rotational levels of the $^2\Pi_{3/2}$ and $^2\Pi_{1/2}$ ionization thresholds.

A weak electrostatic pulse field-ionizes high Rydberg states and accelerates the resulting electrons through the entrance grid which caps a 25 cm long grounded flight tube. The extractor is held at fixed potential off ground, while the repeller is pulsed from a nominal reverse bias of 500 meV/cm to a forward bias of 1 V/cm in 50 ns with a delay of 4 μs. Electrons are collected by a pair of microchannel plates, and the amplified signal is sent to an averaging digital oscilloscope.

Transitions to successive ionization thresholds are marked by the appearance of long-lived Rydberg states of very high principal quantum number ($n>100$) lying just below each ionization threshold. The delayed extraction pulse field ionizes such long-lived states whenever the frequency of the second laser approaches resonance with the threshold. Electrons released by the pulsed field are distinguished from electrons formed directly by their arrival times at the detector.

III. RESULTS

We prepare individual levels of the $4p\pi\ F\ ^1\Delta$, $E\ ^1\Sigma^+$, and $g\ ^3\Sigma^-$ states for subsequent threshold photoionization by rotationally resolved two-photon absorption. Figure 1 shows rotational structure in ionization-detected two-photon absorption transitions which populate these $4p\pi$ Rydberg states with angular momentum quantum numbers $J'=0$, 1, and 2 for $E\ ^1\Sigma^+$ and $g\ ^3\Sigma^-$ states or $J'=3$ and $+/-$ parity components of $J'=2$ for $F\ ^1\Delta$.

Second-laser scans from these two-photon prepared intermediate states probe threshold transitions in the visible to accessible rotational states of HCl^+. Figure 2 shows spectra associated with the $^2\Pi_{3/2}$ and $^2\Pi_{1/2}$ states of HCl^+ obtained by delayed pulsed-field threshold photoionization of the $J'=2$, 1, and 0 levels of the intermediate $E\ ^1\Sigma^+$ state. For the $^2\Pi_{3/2}$ spin–orbit component, we find that the $J^+=\frac{3}{2}$ peak is the strongest in the photoelectron spectra of the $J'=2$ level. The $J^+=\frac{5}{2}$ and $\frac{7}{2}$ peaks are much weaker. Weak $J^+=\frac{5}{2}$ and $\frac{7}{2}$

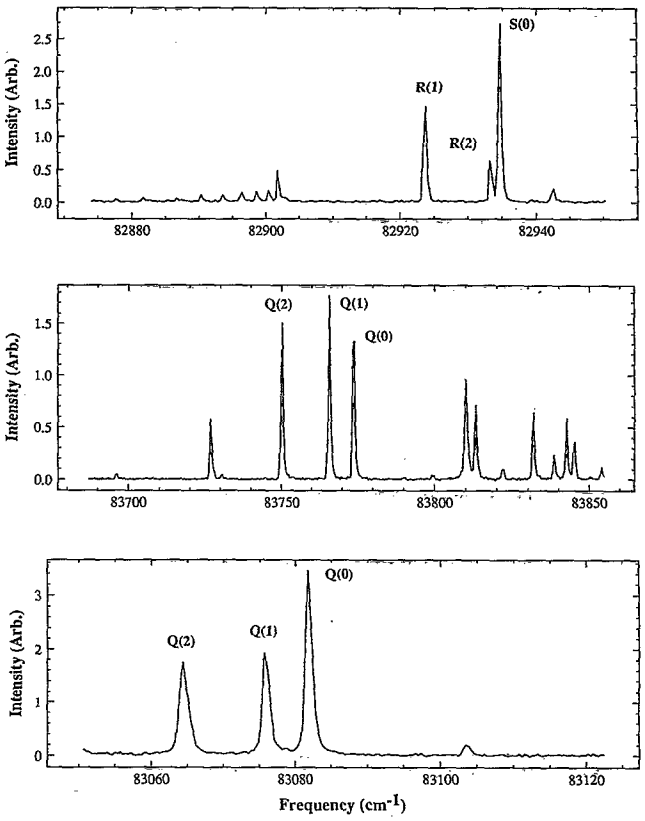

FIG. 1. Ionization-detected two-photon absorption spectra of HCl and DCl showing rotational structure used to select $4p\pi$ intermediate states for double-resonant threshould photoionization. (Upper) $F\ ^1\Delta$ state in DCl; (center) $E\ ^1\Sigma^+$ state in HCl; (lower) $g\ ^3\Sigma^-$ state in HCl.

peaks are also seen from $J'=1$ and $J'=0$, but in both cases $J^+=\frac{3}{2}$ dominates. The lowest rotational levels are also the strongest for threshold photoionization to the $^2\Pi_{1/2}$ manifold, but transitions terminating on higher rotational states are much more evident. Comparing vertical scales in the two parts of Fig. 2, it can be seen that, measured from the $E\ ^1\Sigma^+$ intermediate state, threshold field ionization transitions to the lowest rotational levels display about the same intensity for the $^2\Pi_{3/2}$ and $^2\Pi_{1/2}$ limits.

This is not the case for threshold photoionizing transitions from the $g\ ^3\Sigma^-$ state. Figure 3 shows threshold photoionization spectra from the $J'=0$, 1, and 2 levels of the $g\ ^3\Sigma^-$ state to both spin–orbit ionization limits. Trends in rotational intensities parallel those for the E state; $J^+=\frac{3}{2}$ dominates in the spectrum of the lower spin–orbit component of the ion, while rotational intensities are more broadly distributed for the $^2\Pi_{1/2}$ component. The major difference is in the relative integrated strength of delayed photoionization intensity. Contrary to the pattern established for the E state, photoionization from the g state strongly favors the lower $^2\Pi_{3/2}$ spin–orbit component of the cation, with only relatively weak intensity seen for transitions to the upper spin–orbit state.

The strongest signals observed thus far in the threshold photoionization of HCl have been obtained via intermediate

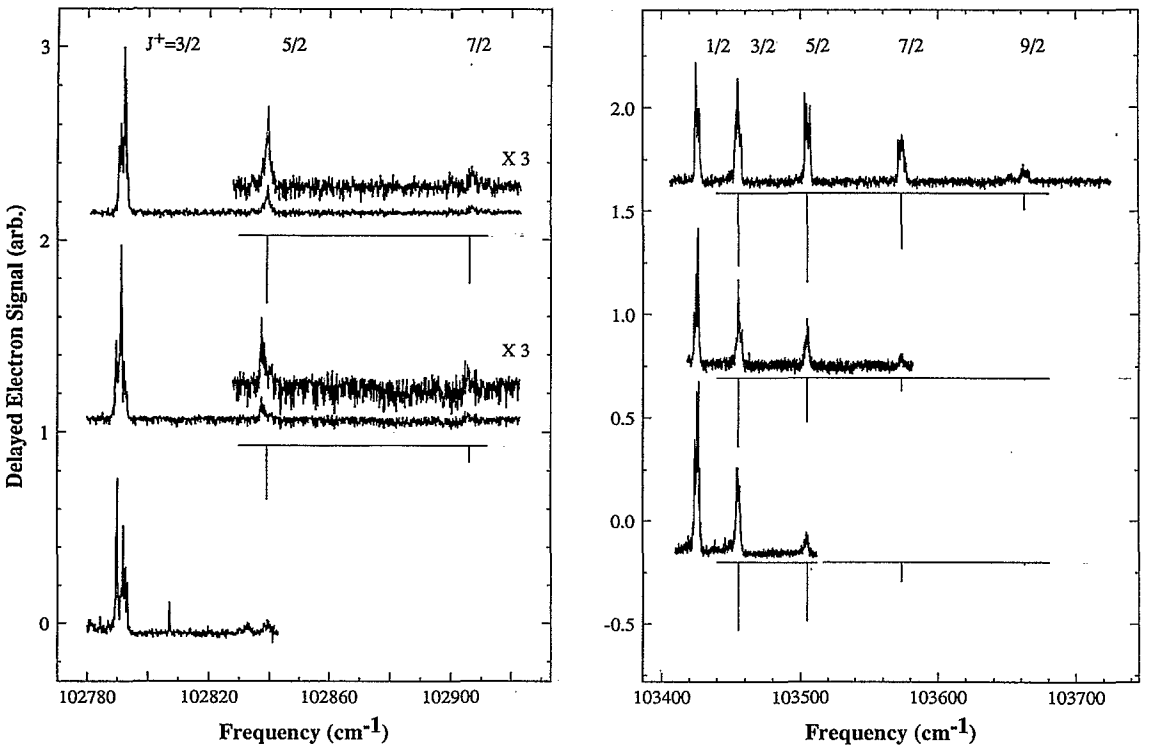

FIG. 2. Delayed pulsed-field threshold photoionization spectra of HCl obtained via intermediate resonance with rotational levels $J'=0$, 1, and 2 of the $E\ ^1\Sigma^+$ ($v=0$) state. Stick spectra show *ab initio* calculated relative intensities, normalized in each case to the first excited J^+ level.

resonance with the $F\ ^1\Delta$ state. Scans taken with DCl show the effect of isotopic substitution. We select rotational levels in DCl using $R(1)$, $R(2)$, and $S(0)$ lines in the spectrum of two-photon transitions from the ground state (see Fig. 1). Figure 4 shows threshold photoionization scans over the $^2\Pi_{3/2}$ and $^2\Pi_{1/2}$ thresholds for each of these intermediate levels. Observed rotational intensities, for the most part, parallel those found for threshold photoionization of HCl via the $F\ ^1\Delta$ state. Overall intensities for transitions to the lower spin–orbit state of the cation are somewhat greater than those to the upper component, and in most cases the lowest accessible rotational state for each component displays the largest delayed pulsed-field ionization signal. However, the higher rotational thresholds ($J^+=\frac{7}{2}$ and $\frac{9}{2}$) of the $^2\Pi_{3/2}$ component are noticeably enhanced for DCl compared to HCl, and, in the scan from $J'=3$ over the $^2\Pi_{1/2}$ threshold, the envelope of rotational transitions peaks at $J^+=\frac{5}{2}$.

IV. DISCUSSION

A. Energy positions of the lines

Threshold photoionization spectra yield ionization potentials for specific rotational levels of HCl^+ and DCl^+. Correcting for field effects, the results obtained here agree well with thresholds recently observed in XUV transitions from the ground state of HCl by Tonkyn *et al.*[15] and established earlier by Rydberg extrapolations.[7,8] The lowest ionization potential of DCl is 40 cm^{-1} higher than that for HCl due to zero-point differences, in agreement with the results of Natalis *et al.*[16] The energy intervals between rotational levels agree with those derived from the constants obtained by Lubic *et al.*[17]

B. Rotational line intensities

To examine trends theoretically for the broader set of intermediate states studied here, we have carried out two different calculations, following very similar techniques. The first calculation uses the same approach as described in Ref. 18. The $4p\pi$ Rydberg orbital is approximated by the first virtual orbital of the self-consistent-field (SCF) solution for the $X\ ^2\Pi$ ion core.[19] The basis set consists of five diffuse Slater orbitals on the center of mass ($4p\pi$ $\zeta=0.59$, $4p\pi$ $\zeta=0.26$, $3d\pi$ $\zeta=0.357$, $4d\pi$ $\zeta=0.257$, and $4f\pi$ $\zeta=0.333$). The energy of the $F\ ^1\Delta$ state in this approximation is -459.763 a.u. at $R=2.409a_0$. Continuum orbitals with up to $l=3$ are obtained in the static exchange frozen-core approximation[20] for a photoelectron energy of 0.005 a.u.

The other calculation uses multiplet-specific final state wave functions in a Hartree–Fock frozen-core approximation and an intermediate coupling scheme between Hund's cases (a) and (b) for the $^2\Pi$ ion. The photoelectron orbitals were obtained by numerical solution of the associated Lippmann–Schwinger equations using an iterative procedure, based on the Schwinger variational principle;[21] details are given elsewhere.[9] The main difference between this method and that just described is that the basis set in the second case uses Gaussian orbitals in place of Slater orbitals, but the energy for the $F\ ^1\Delta$ state is very similar: -459.755

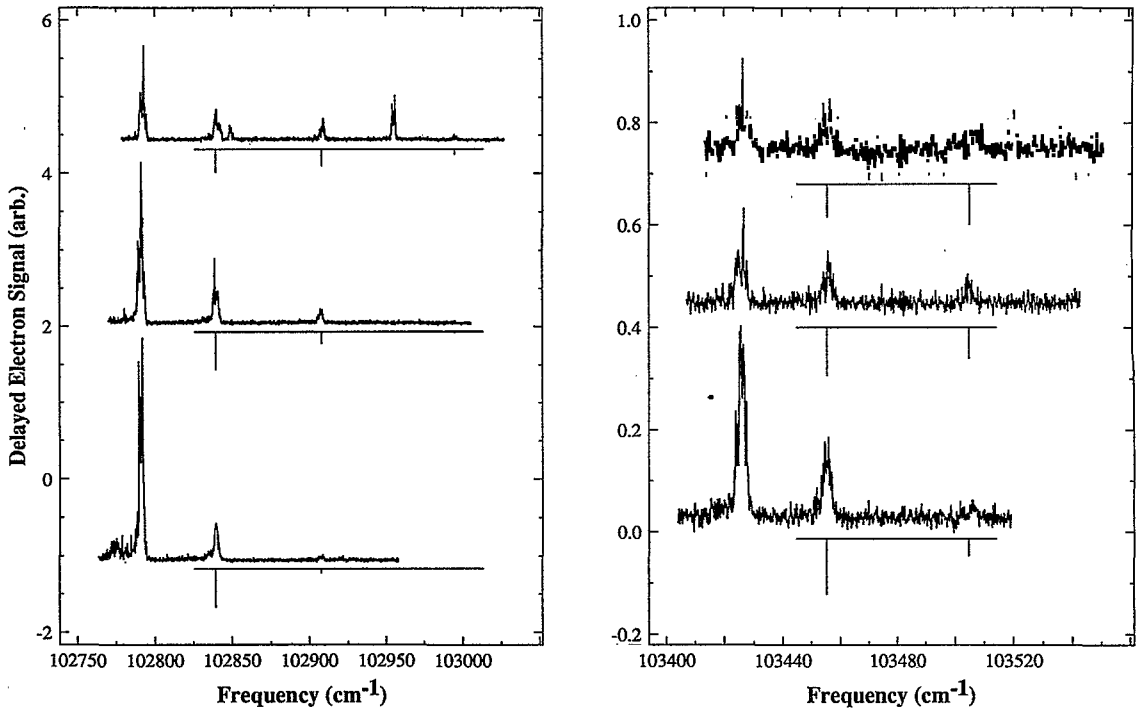

FIG. 3. Delayed pulsed-field threshold photoionization spectra of HCl obtained via intermediate resonance with rotational levels $J'=0$, 1, and 2 of the $g\ ^3\Sigma^-$ ($v=0$) state. Stick spectra show *ab initio* calculated relative intensities, normalized in each case to the first excited J^+ level.

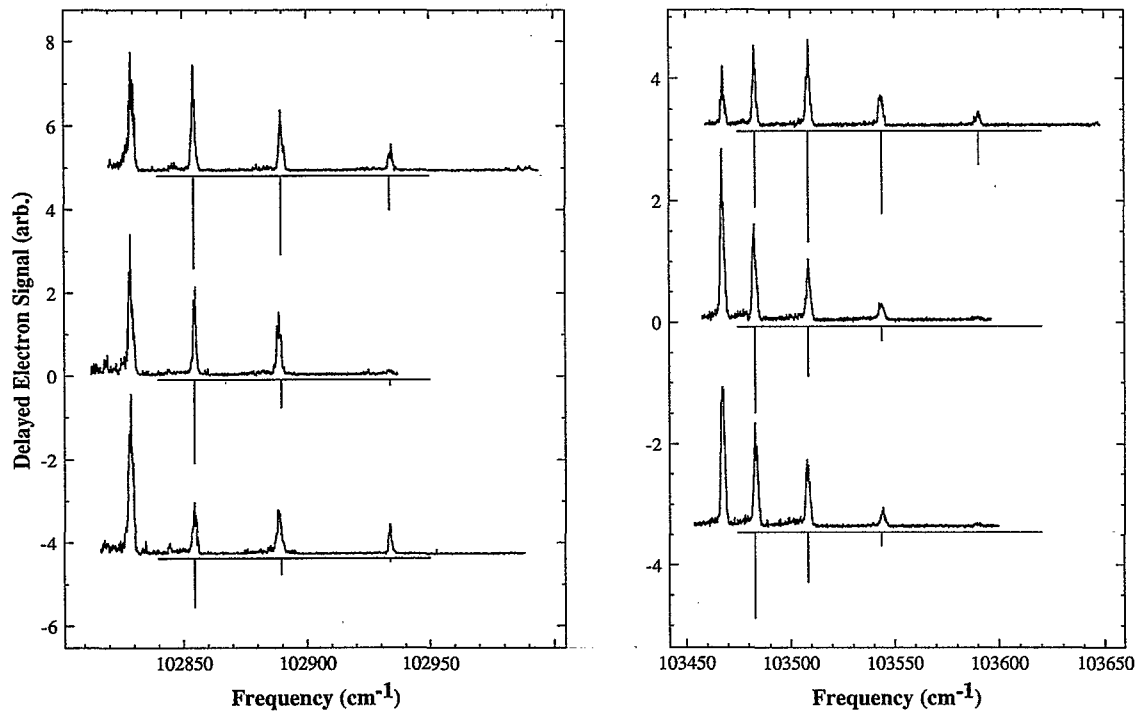

FIG. 4. Delayed pulsed-field threshold photoionization spectra of DCl obtained via intermediate resonance with rotational levels $J'=0$, 1, and 2 of the $F\ ^1\Delta$ ($v=0$) state. Stick spectra show *ab initio* calculated relative intensities, normalized in each case to the first excited J^+ level.

a.u. at $R=2.484a_0$. Note that the rotationally resolved photoelectron spectra should be the same for both methods if the basis set used to describe the continuum orbitals is complete. The $4p\pi$ Rydberg orbital is taken as different for singlet and triplet states (though we can assume, and calculations appear to confirm, that transition moments for triplet-discrete to triplet-continuum transitions are very close to those obtained from corresponding singlet-discrete to singlet-continuum states). Single-center expansion of these $4p\pi$ orbitals around its center-of-mass shows that it has 95.25% p, 4.70% d, and 0.04% f character for the $F\ ^1\Delta$ state at the R_e of $2.484a_0$, 96.28% p, 3.71% d, and 0.02% f character for the $E\ ^1\Sigma^+$ state at the $R_e=2.51a_0$, and 95.50% p, 4.44% d, and 0.05% f character for the $g\ ^3\Sigma^-$ state at the $R_e=2.436a_0$. This calculation also introduces the effect of alignment in photopreparation of the F and E intermediate states.

The predicted photoelectron spectra are very similar for both methods. We tabulate the results of our calculations in Tables I–III for rotational branching ratios corresponding to schemes used in the measured spectra for the $F\ ^1\Delta$, $E\ ^1\Sigma^+$, and $g\ ^3\Sigma^-$ Rydberg states, respectively. Since the photoelectron continuum is not expected to be influenced by isotopic substitution, the calculations for the $F\ ^1\Delta$ state of DCl use the same photoelectron matrix elements as for photoionization of the $F\ ^1\Delta$ state of HCl. We therefore expect the photoionization dynamics for the DCl to be similar to that of HCl. The rotational branching ratios for the $S(0)$ branch of the $F\ ^1\Delta$ state of DCl (Fig. 4) are indeed very close to those of HCl (Refs. 8 and 9).

Comparison of the calculated intensities with measured values shows that in every case the experimental peak for the lowest rotational level in each spin–orbit component is disproportionally intense. This is particularly evident for transitions to the lower $^2\Pi_{3/2}$ state of HCl^+. While clearly anomalous, such behavior is not unexpected based on comparison with other threshold spectra measured by delayed pulsed-field ionization. In spectra of NO_2, N_2O, and NO, as well as for specific cases in the spectrum of H_2 and N_2,[22] and in HCl itself observed in XUV transitions from the neutral ground state, discrete–discrete rotational interactions enhance transitions to final states of lowest accessible rotational quantum number.[15,23,24]

The $J^+=\frac{3}{2}$ level of HCl^+ ($^2\Pi_{3/2}$), in particular, is special in that underlying Rydberg states of lower principal quantum number converging to higher rotational thresholds that can lend intensity through such discrete–discrete interactions can only decay through predissociation and radiation; before application of the pulsed field they cannot autoionize. Discrete states underlying higher rotational thresholds can rotationally autoionize in the case of the $^2\Pi_{3/2}$ substate and spin orbit as well as rotationally autoionize in the case of the $^2\Pi_{1/2}$ substate. As discussed later, the availability of such decay channels appears to moderate discrete–discrete intensity transferring interactions. For this reason, we do not include initial rotational levels $J^+=\frac{1}{2}$ for the $^2\Pi_{1/2}$ ion and $J^+=\frac{3}{2}$ for $^2\Pi_{3/2}$ in comparing our calculated spectra with experimental intensities in Figs. 2–4. The results of such comparison seem to support this idea. Figures 2–4 include stick spectra indicating calculated relative intensities derived for threshold photoionizing transitions to the excited rotational levels. Comparison of the calculated rotational intensities of Tables I–III, obtained on the basis of direct ionization only, with the measured spectra shown in Figs. 2–4 illustrates well the effects of autoionization on these threshold photoionization spectra. For transitions originating in the $E\ ^1\Sigma^+$ state and terminating in the upper spin–orbit component (Fig. 2), the agreement appears especially good. Spectra for the lower spin–orbit component are relatively weak for this intermediate state, and quantitative comparison is difficult.

TABLE I. Relative intensities computed for rotationally detailed threshold photoionizing transitions to $HCl^+\ ^2\Pi_{3/2}$ and $^2\Pi_{1/2}$ from rotational states J' of the $4p\pi\ F\ ^1\Delta$ Rydberg state (for an aligned intermediate state).

$^2\Pi_{3/2}$		$^2\Pi_{1/2}$	
$J'=2,S(0)$ line			
		$J^+=\frac{1}{2}$	1.00
$J^+=\frac{3}{2}$	1.00	$\frac{3}{2}$	0.81
$\frac{5}{2}$	0.35	$\frac{5}{2}$	0.46
$\frac{7}{2}$	0.21	$\frac{7}{2}$	0.20
$\frac{9}{2}$	0.03	$\frac{9}{2}$	0.03
$J'=2,R(1)$ line			
		$J^+=\frac{1}{2}$	1.00
$J^+=\frac{3}{2}$	1.00	$\frac{3}{2}$	0.98
$\frac{5}{2}$	0.48	$\frac{5}{2}$	0.59
$\frac{7}{2}$	0.22	$\frac{7}{2}$	0.23
$\frac{9}{2}$	0.03	$\frac{9}{2}$	0.04
$J'=3,R(2)$ line			
		$J^+=\frac{1}{2}$	0.22
$J^+=\frac{3}{2}$	0.47	$\frac{3}{2}$	0.77
$\frac{5}{2}$	1.00	$\frac{5}{2}$	1.00
$\frac{7}{2}$	0.82	$\frac{7}{2}$	0.78
$\frac{9}{2}$	0.44	$\frac{9}{2}$	0.35
$\frac{11}{2}$	0.09	$\frac{11}{2}$	0.07

Due to our assumption of the equivalence of triplet–triplet and singlet–singlet transition moments, the calculated rotational intensities are the same for threshold photoionizing transitions originating in the $g\ ^3\Sigma^-$ state. The pattern of intensities for transitions terminating above the lowest rotational state indeed resemble those observed from $E\ ^1\Sigma^+$, to the extent that signal levels make such comparisons meaningful. This reflects the fact that the angular momentum components of the photoelectron are similar for photoionization of the $4p\pi$ orbitals of the E and g states since both have almost pure p (~96%) character.

In previous experimental studies of HCl, the resonant intermediate $J'=2$ level of the $F\ ^1\Delta$ state was accessed via the $S(0)$ branch.[8] Theoretical methods have also been applied to this system.[9] For transitions to the $^2\Pi_{1/2}$ limit, the most intense peak in the calculated spectra was for $\Delta N=0$,[25] with inclusion of alignment in the resonant state, and $\Delta N=-1$ ($J^+=\frac{1}{2}$) upon introduction of alignment.[9] For the $^2\Pi_{3/2}$ component, calculations with and without alignment both give $\Delta N=-1$ as the most intense peak. The same behavior occurs

TABLE II. Relative intensities computed for rotationally detailed threshold photoionizing transitions to HCl^+ $^2\Pi_{3/2}$ and $^2\Pi_{1/2}$ from rotational states J' of the $4p\pi$ E $^1\Sigma^+$ Rydberg state (for an aligned intermediate state).

$^2\Pi_{3/2}$		$^2\Pi_{1/2}$	
	$J'=0, Q(0)$ line		
		$J^+=\frac{1}{2}$	0.95
$J^+=\frac{3}{2}$	1.00	$\frac{3}{2}$	1.00
$\frac{5}{2}$	0.51	$\frac{5}{2}$	0.46
$\frac{7}{2}$	0.10	$\frac{7}{2}$	0.08
	$J'=1$, $Q(1)$ line		
		$J^+=\frac{1}{2}$	0.84
$J^+=\frac{3}{2}$	1.00	$\frac{3}{2}$	1.00
$\frac{5}{2}$	0.67	$\frac{5}{2}$	0.71
$\frac{7}{2}$	0.33	$\frac{7}{2}$	0.29
$\frac{9}{2}$	0.06	$\frac{9}{2}$	0.04
	$J'=2$, $Q(2)$ line		
		$J^+=\frac{1}{2}$	0.37
$J^+=\frac{3}{2}$	0.61	$\frac{3}{2}$	0.95
$\frac{5}{2}$	1.00	$\frac{5}{2}$	1.00
$\frac{7}{2}$	0.67	$\frac{7}{2}$	0.69
$\frac{9}{2}$	0.36	$\frac{9}{2}$	0.28
$\frac{11}{2}$	0.06	$\frac{11}{2}$	0.04

for photoionization of the F $^1\Delta$ state of DCl (see Fig. 4). Furthermore, the measured and calculated spectra for the $J'=3$ level of the F $^1\Delta$ [$R(2)$ branch] state of DCl in Fig. 4 show that the most intense peaks in the spectra of the $^2\Pi_{1/2}$ cation is $J^+=\frac{5}{2}$, corresponding to $N^+=3$ or $\Delta N=0$. Similar behavior is also predicted for photoionization of the F $^1\Delta$ ($5p\pi$) Rydberg state of HBr.[26]

TABLE III. Relative intensities computed for rotationally detailed threshold photoionizing transitions to HCl^+ $^2\Pi_{3/2}$ and $^2\Pi_{1/2}$ from rotational states J' of the $4p\pi$ g $^3\Sigma^-$ Rydberg state (for an aligned intermediate state).

$^2\Pi_{3/2}$		$^2\Pi_{1/2}$	
	$J'=0, Q(0)$ line		
		$J^+=\frac{1}{2}$	1.00
$J^+=\frac{3}{2}$	1.00	$\frac{3}{2}$	0.66
$\frac{5}{2}$	0.47	$\frac{5}{2}$	0.37
$\frac{7}{2}$	0.12	$\frac{7}{2}$	0.04
	$J'=1, Q(1)$ line		
		$J^+=\frac{1}{2}$	0.97
$J^+=\frac{3}{2}$	1.00	$\frac{3}{2}$	1.00
$\frac{5}{2}$	0.46	$\frac{5}{2}$	0.45
$\frac{7}{2}$	0.11	$\frac{7}{2}$	0.11
$\frac{9}{2}$	0.01	$\frac{9}{2}$	0.01
	$J'=2, Q(2)$ line		
		$J^+=\frac{1}{2}$	0.39
$J^+=\frac{3}{2}$	0.66	$\frac{3}{2}$	0.97
$\frac{5}{2}$	1.00	$\frac{5}{2}$	1.00
$\frac{7}{2}$	0.58	$\frac{7}{2}$	0.48
$\frac{9}{2}$	0.15	$\frac{9}{2}$	0.12
$\frac{11}{2}$	0.02	$\frac{11}{2}$	0.01

For transitions from the F $^1\Delta$ state in DCl where signal levels are highest, calculated intensities can be compared with experimental ones for many more transitions. Note that the F $^1\Delta$ state is also perturbed by the b $^3\Pi$ and C $^1\Pi$ states[27] but these small effects have been neglected in the calculations. Agreement between these calculated and measured spectra is quite reasonable with the exception of higher rotational levels of the $^2\Pi_{3/2}$ substate, where the measured relative intensities are noticeably enhanced compared to theoretical predictions and to corresponding intensities observed in the threshold photoionization spectrum of HCl.[8] We suggest that these intensity anomalies for DCl arise from discrete–discrete intensity sharing interactions with underlying Rydberg states converging to the upper spin–orbit component. When isoenergetic with Rydberg levels near threshold, such states can form long-lived complex resonances with absorption cross sections that are enhanced by the low principal quantum number of the interloper (serving in this case to counteract the broader intensity decreasing effect of the discrete-continuum rotational autoionizing interaction).

Double-resonant spin–orbit autoionizing studies show that the spectrum of candidate states is dense for DCl.[28] For example, multichannel quantum defect theory (MQDT) calculations suggest that the position of the $^2\Pi_{3/2}$ $J^+=\frac{7}{2}$ rotational level coincides with a long-lived $l=4$ autoionizing resonance with principal quantum number $n=12$ in the series converging to $J^+=\frac{11}{2}$ of the $^2\Pi_{1/2}$ substate.[29] The corresponding resonance has been observed in the delayed autoionization spectrum of HCl,[8] but it does not coincide with any rotational threshold of the $^2\Pi_{3/2}$ substate. In general, MQDT calculations find more coincidences between rotational thresholds and interloping Rydberg states for DCl than HCl. This probably reflects the smaller rotational constant for DCl which gives rise to more rotational perturbations and consequently a more uniform distribution of discrete Rydberg states.

We thus have a pattern of intensities in which first rotational levels appear enhanced, particularly for the lower spin–orbit substate, while higher thresholds appear to be in at least qualtitative agreement with simple theoretical linestrength expectations (apart from specific perturbations). This fits well with a general picture of the effect of rapid decay channels on intensities in delayed pulsed-field threshold photoionization spectroscopy which can best be seen by looking at the relative intensities of spin–orbit components.

C. Intensities of transitions to the spin–orbit substates of HCl^+

The intensities of the ion rotational distributions associated with the two cation substates convey information on the electronic character of the intermediate state. Theoretically, if the intermediate state has pure singlet (or triplet) character and the ion core is treated in pure Hund's case (a), the total intensities for the $^2\Pi_{1/2}$ and $^2\Pi_{3/2}$ thresholds will be equal. However, it is worth noting that conventional photoelectron spectra out of the X $^1\Sigma^+$ ground state of HCl (Refs. 16 and

30) and HF (Ref. 31) show a slightly stronger intensity for the $^2\Pi_{3/2}$ component. Recent theoretical investigations, assuming an intermediate coupling scheme between Hund's cases (a) and (b) for the $^2\Pi$ ion,[32] reproduce well the measured intensity ratio of 1.20 for the spin–orbit components of the ion observed in photoionization of HF.[31] The calculated intensity ratio[33] of 1.06 is also in excellent agreement with the measured value of 1.06 ± 0.05 for HCl.[30] For resonant Rydberg states, it is well known that singlet and triplet states with the same Rydberg orbital can be strongly mixed by the spin–orbit interaction (see, for example, Ref. 34). If this mixing is complete, only one substate is accessible by photoionization. This is the case for experiments on HBr,[35] where the intermediate state, $F\ ^1\Delta_2$, can be described purely in terms of Hund's case (c) as a complete mixture of the $^1\Delta_2$ and $^3\Delta_2$ states from the $5p\pi$ Rydberg configuration. In this case, the core of the $F\ ^1\Delta_2$ state has the spin–orbit configuration $^2\Pi_{1/2}$. Photoionization from this state populates only the $^2\Pi_{1/2}$ component of the cation. In HCl, the spin–orbit singlet-triplet mixing of the $4p\pi$ configuration is not complete. Starting from $F\ ^1\Delta_2$, the conventional photoelectron spectra of de Beer *et al.*[10,36] show a $^2\Pi_{1/2}/^2\Pi_{3/2}$ ratio of about 6.5, which corresponds to a singlet-triplet mixing of 22%, as estimated recently.[37] Further studies by de Beer *et al.*[10] also confirm that this ratio is insensitive to the photoelectron energy.

This value of the spin–orbit branching ratio is not seen in rotationally resolved threshold photoionization spectra of HCl recorded in transitions from the $F\ ^1\Delta$ state by delayed pulsed-field threshold photoionization. For example, in the case of the $F\ ^1\Delta$ ($J'=3$) state in DCl, which is typical, the experimental ratio summed over all rotational lines is $I(^2\Pi_{1/2})/I(^2\Pi_{3/2})=0.56$. This is opposite to the trend observed in conventional photoelectron spectrum. This discrepancy, together with anomalous rotational intensities, can be seen to be due to rotational coupling and spin–orbit autoionization.

Delayed pulsed-field threshold photoionization spectroscopy relies on the long lifetimes of high Rydberg states lying just below the ionization threshold for each state of the ion. Any factors shortening the lifetimes of such states affect the spectrum by reducing the population of neutral states available for field ionization after a given delay and thereby diminishing intensities. All high Rydberg states converging to the $^2\Pi_{1/2}$ limit of HCl^+ can autoionize via spin–orbit coupling to the $^2\Pi_{3/2}$ continuum. Series of different l can be expected to have different rates of autoionization and, indeed, we have found evidence for very long-lived series with near-zero quantum defect.[8] Nevertheless, the accessibility of channels for decay by autoionization can do nothing but shorten the lifetimes of these near-threshold states, and apparently do so by enough to account for a systematic decrease in intensity for threshold photoionization from the $F\ ^1\Delta$ state to the upper spin–orbit component.

Rydberg states converging to rotational levels of the lower spin–orbit component can rotationally autoionize, except for those built on the lowest such state $J^+=\frac{3}{2}$. Indeed, as noted earlier, in every case this lowest ionization limit gives rise to the most intense threshold transition in the $^2\Pi_{3/2}$ substate, often in contrast to theoretical predictions of rotational propensities favoring higher rotational levels of the cation. Interestingly, for the upper spin–orbit component where all levels can autoionize by spin–orbit coupling, the lowest rotational level is not so favored in delayed pulsed-field threshold photoionization, and experimental intensities approach theoretically predicted values. This suggests a zeroth-order model which recognizes the special character of the lowest rotational state of the cation, and then groups levels with open autoionization channels as having decreased intensity in proportion to their absorption cross sections. Refinements to this picture will distinguish between rotational and spin–orbit autoionization, recognize possible J^+ dependencies[38] and include neutral continua (predissociation).

The spectrum of threshold photoionizing transitions from the $4p\pi\ g\ ^3\Sigma^-$ intermediate state provides a further opportunity to examine the combined effects of intermediate photoselection and final-state dynamics on spin–orbit and rotational intensities. Summing over ion rotational levels for ionization of the $J=0$ level, the ratio of spin–orbit intensities, $^2\Pi_{1/2}/^2\Pi_{3/2}$, is 0.18, which is considerably smaller than observed for singlet intermediate states. This ratio, which also holds for higher total angular momentum resonant levels, is in line with expectations based on the computed extent of singlet-triplet mixing in the $4p\pi$ configuration. Thus, if threshold photoionization intensities measured by delayed pulsed-field ionization can be equated with cross sections for direct ionization, then the spin–orbit ratios observed can be associated with the following electronic wave function for the $4p\pi\ g\ ^3\Sigma^-$ Rydberg state:

$$0.925\ ^3\Sigma^- + 0.38\ ^1\Sigma^+.$$

However, we know that the intensity of the $^2\Pi_{1/2}$ threshold structure observable experimentally is reduced by spin–orbit autoionization. Furthermore, the strong variation with vibrational quantum number in the coupling between $E\ ^1\Sigma^+$ and $g\ ^3\Sigma^-$ (Ref. 1), and the anomalous rotational constant of this state suggest a strong mixing of $E\ ^1\Sigma^+$ with the $V\ ^1\Sigma^+$ valence state. The combination of these factors suggest that the direct interpretation of the observed threshold photoionization spectrum in terms of a simple two-state description of spin–orbit coupling in the $4p\pi$ Rydberg manifold cannot be correct. More quantitative analysis of the significance of the intensity ratios for this case must await a fuller characterization of the state together with a more quantitative understanding of the effect of spin–orbit autoionization on delayed threshold photoionization intensities.

In conclusion, comparison of state-selected threshold photoionization intensities with *ab initio* calculations as well as with available photoelectron spectra confirm suggestions made by Lefebvre-Brion[11] and de Beer *et al.*[10] that spin–orbit autoionization reduces intensities in delayed pulsed-field threshold photoionization of HCl. Discrete-continuum interactions also appear to have the further effect of moderating discrete–discrete intensity (lifetime) sharing rotational interactions. It would thus appear important in the analysis of intensities in pulsed-field threshold photoionization to include effects of discrete-continuum interactions on dynamics associated with the detection process. It would also be useful

for experiment to obtain absolute cross sections for delayed threshold electron production to compare with theoretical estimates based on direct ionization.

ACKNOWLEDGMENTS

Work at Purdue was supported by the National Science Foundation and CNRS (NSF Grant Nos. CHE-9307131 and INT-9216810). Work at California Institute of Technology was supported by grants from the Air Force Office of Scientific Research and the Office of Health and Environmental Research of the U.S. Department of Energy. V.M. and K.W. also acknowledge use of resources of the Jet Propulsion Laboratory/California Institute of Technology CRAY Y-MP2E/232 Supercomputer.

[1] S. G. Tilford, M. L. Ginter, and J. T. Vanderslice, J. Mol. Spectrosc. **33**, 505 (1970); S. G. Tilford and M. L. Ginter, *ibid.* **40**, 568 (1971); D. T. Terwilliger and A. L. Smith, *ibid.* **45**, 366 (1973); J. Chem. Phys. **63**, 1008 (1975); D. S. Ginter and M. L. Ginter, J. Mol. Spectrosc. **90**, 177 (1981).
[2] M. Bettendorff, S. D. Peyerimhoff, and R. J. Buenker, Chem. Phys. **66**, 261 (1982).
[3] S. Arepalli, N. Presser, D. C. Robie, and R. J. Gordon, Chem. Phys. Lett. **118**, 88 (1985); R. Callaghan, S. Arepalli, and R. J. Gordon, J. Chem. Phys. **86**, 5273 (1987).
[4] D. S. Green, G. A. Bickel, and S. C. Wallace, J. Mol. Spectrosc. **150**, 303 (1991); **150**, 354 (1991); **150**, 388 (1991); D. S. Green and S. C. Wallace, J. Chem. Phys. **96**, 5857 (1992).
[5] T. A. Spiglanin, D. W. Chandler, and D. H. Parker, Chem. Phys. Lett. **137**, 414 (1987).
[6] A. J. Yencha, D. Kaur, R. J. Donovan, A. Kvaran, A. Hopkirk, H. Lefebvre-Brion, and F. Keller, J. Chem. Phys. **99**, 4986 (1993).
[7] K. S. Haber, E. Patsilinakou, Y. Jiang, and E. R. Grant, J. Chem. Phys. **94**, 3429 (1991).
[8] K. S. Haber, G. Bryant, Y. Jiang, E. R. Grant, and H. Lefebvre-Brion, Phys. Rev. A **44**, R5331 (1993).
[9] K. Wang and V. McKoy, J. Chem. Phys. **95**, 8718 (1991).
[10] E. de Beer, W. J. Buma, and C. A. de Lange, J. Chem. Phys. **99**, 3252 (1993).
[11] H. Lefebvre-Brion, in *Proceedings of the International Workshop on Photoionization,* Berlin, 1992, edited by U. Becker and U. Heinzmann (AMS, New York, 1993), p. 123.
[12] F. Merkt and T. P. Softley, Int. Rev. Phys. Chem. **12**, 205 (1993), and references therein.
[13] F. Merkt, S. R. Mackenzie, R. J. Rednall, and T. P. Softley, J. Chem. Phys. **99**, 8430 (1993).
[14] K. Müller-Dethlefs, M. S. Sander, and E. W. Schlag, Z. Naturforsch. Teil A **39**, 1089 (1984).
[15] R. G. Tonkyn, R. T. Wiedmann, and M. G. White, J. Chem. Phys. **96**, 3696 (1992).
[16] P. Natalis, P. Pennetreau, L. Lonton, and J. E. Collin, Chem. Phys. **73**, 191 (1982).
[17] K. G. Lubic, D. Ray, D. C. Hovde, L. Veseth, and R. J. Saykally, J. Mol. Spectrosc. **134**, 1 (1989).
[18] H. Lefebvre-Brion, Chem. Phys. Lett. **171**, 377 (1990).
[19] H. Lefebvre-Brion and C. M. Moser, J. Mol. Spectrosc. **13**, 418 (1964).
[20] G. Raseev, H. Le Rouzo, and H. Lefebvre-Brion, J. Chem. Phys. **72**, 5701 (1980).
[21] R. R. Lucchese, G. Raseev, and V. McKoy, Phys. Rev. A **25**, 2572 (1982).
[22] F. Merkt and T. P. Softley, J. Chem. Phys. **96**, 4149 (1992); F. Merkt and T. P. Softley, Phys. Rev. A **46**, 302 (1992).
[23] R. T. Wiedmann, E. R. Grant, R. G. Tonkyn, and M. G. White, J. Chem. Phys. **95**, 746 (1991).
[24] G. P. Bryant, Y. Jiang, M. Martin, and E. R. Grant, J. Phys. Chem. **96**, 6875 (1992).
[25] H. Lefebvre-Brion (unpublished).
[26] K. Wang and V. McKoy, J. Chem. Phys. **95**, 7872 (1991).
[27] R. Liyanage, P. T. A. Reilly, Y.-A. Yang, R. J. Gordon, and R. W. Field, Chem. Phys. Lett. **216**, 544 (1993).
[28] Y.-F. Zhu, E. R. Grant, and H. Lefebvre-Brion, J. Chem. Phys. **99**, 2287 (1993).
[29] H. Lefebvre-Brion (unpublished).
[30] A. J. Yencha, J. Ganz, M.-W. Ruf, and H. Hotop, Z. Phys. D **14**, 57 (1989).
[31] K. Wang, V. McKoy, M.-W. Ruf, A. J. Yencha, and H. Hotop, J. Elect. Spectrosc. Rel. Phen. **63**, 11 (1993); A. J. Yencha, M.-W. Ruf, and H. Hotop, Z. Phys. D **27**, 131 (1993).
[32] K. Wang and V. McKoy, J. Chem. Phys. **95**, 4977 (1991).
[33] K. Wang and V. McKoy (unpublished).
[34] H. Lefebvre-Brion, A. Giusti-Suzor, and G. Raseev, J. Chem. Phys. **83**, 1557 (1986).
[35] J. Xie and R. N. Zare, Chem. Phys. Lett. **159**, 399 (1989); private communication.
[36] E. de Beer, B. G. Koenders, M. P. Koopmans, and C. A. de Lange, J. Chem. Soc. Faraday Trans. **86**, 2038 (1990).
[37] Y. Xie, P. T. A. Reilly, S. Chilukuri, and R. J. Gordon, J. Chem. Phys. **95**, 854 (1991).
[38] H. Lefebvre-Brion (unpublished).